Connecting polymer collapse and the onset of jamming

Alex T. Grigas [1,2] Aliza Fisher,[3] Mark D. Shattuck [4] and Corey S. O'Hern [3,1,2,5,6]

[1]*Graduate Program in Computational Biology and Bioinformatics, Yale University, New Haven, Connecticut 06520, USA*
[2]*Integrated Graduate Program in Physical and Engineering Biology, Yale University, New Haven, Connecticut 06520, USA*
[3]*Department of Mechanical Engineering and Materials Science, Yale University, New Haven, Connecticut 06520, USA*
[4]*Benjamin Levich Institute and Physics Department, The City College of New York, New York, New York 10031, USA*
[5]*Department of Physics, Yale University, New Haven, Connecticut 06520, USA*
[6]*Department of Applied Physics, Yale University, New Haven, Connecticut 06520, USA*

(Received 16 September 2023; accepted 13 February 2024; published 18 March 2024)

Previous studies have shown that the interiors of proteins are densely packed, reaching packing fractions that are as large as those found for static packings of individual amino-acid-shaped particles. How can the interiors of proteins take on such high packing fractions given that amino acids are connected by peptide bonds and many amino acids are hydrophobic with attractive interactions? We investigate this question by comparing the structural and mechanical properties of collapsed attractive disk-shaped bead-spring polymers to those of three reference systems: static packings of repulsive disks, of attractive disks, and of repulsive disk-shaped bead-spring polymers. We show that the attractive systems quenched to temperatures below the glass transition $T \ll T_g$ and static packings of both repulsive disks and bead-spring polymers possess similar interior packing fractions. Previous studies have shown that static packings of repulsive disks are isostatic at jamming onset, i.e., the number of interparticle contacts N_c matches the number of degrees of freedom, which strongly influences their mechanical properties. We find that repulsive polymer packings are hypostatic at jamming onset (i.e., with fewer contacts than degrees of freedom) but are effectively isostatic when including stabilizing quartic modes, which give rise to quartic scaling of the potential energy with displacements along these modes. While attractive disk and polymer packings are often considered hyperstatic with excess contacts over the isostatic number, we identify a definition for interparticle contacts for which they can also be considered as effectively isostatic. As a result, we show that the mechanical properties (e.g., scaling of the potential energy with excess contact number and low-frequency contribution to the density of vibrational modes) of weakly attractive disk and polymer packings are similar to those of *isostatic* repulsive disk and polymer packings. Our results demonstrate that static packings generated via attractive collapse or compression of repulsive particles possess similar structural and mechanical properties.

DOI: 10.1103/PhysRevE.109.034406

I. INTRODUCTION

It has long been appreciated since the first atomic-resolution x-ray crystal structures of proteins were solved that their interior, solvent-inaccessible, or core, regions are densely packed, regardless of the differences in their overall folds [1–6]. Other experimental atomic-scale structural characterization methods, such as NMR spectroscopy, provide all-atom structures of proteins in solution and at room temperature and have shown that high-quality NMR structures also possess densely packed interiors with packing fractions similar to those of x-ray crystal structures [7]. Perturbing the dense packing of the solvent-inaccessible hydrophobic interior of proteins via amino acid mutations has been shown to significantly affect protein structure and stability [8–11]. In addition, the properties of protein core packing have been used to predict the accuracy of the overall fold in computational protein structure prediction [12].

Prior analyses of protein x-ray crystal structures that allowed unphysical atomic overlaps suggested that the interiors of proteins possessed packing fractions as large as $\phi \sim 0.7$–0.75 [1,5]. However, more recent studies that account for the nonspherical shapes of amino acids and do not allow atomic overlaps have shown that the average packing fraction of solvent-inaccessible amino acids is $\phi \approx 0.55 \pm 0.02$ [6,13–15]. Why do the core regions of all experimentally determined protein structures, regardless of the overall fold, possess this value for the packing fraction? Previously, we have shown that jammed packings of rigid amino-acid-shaped particles with purely repulsive interactions under periodic boundary conditions possess similar packing fraction distributions as those for experimentally determined protein cores [6]. Despite this agreement, these prior simulations lacked important features of protein structure: The amino acids were rigid with no backbone dihedral angle degrees of freedom and they were *disconnected*, lacking peptide bonds; the packings were generated by compression, not by hydrophobic polymer collapse; and the packings were generated using periodic boundary conditions instead of being fully solvated. In addition, when thermal fluctuations are included in the amino-acid-shaped particle-packing generation protocol, we find that the onset of jamming occurs over a range of packing fractions, $0.55 \lesssim \phi_J \lesssim 0.62$, where ϕ_J increases as the rate at which thermal energy is removed from the system

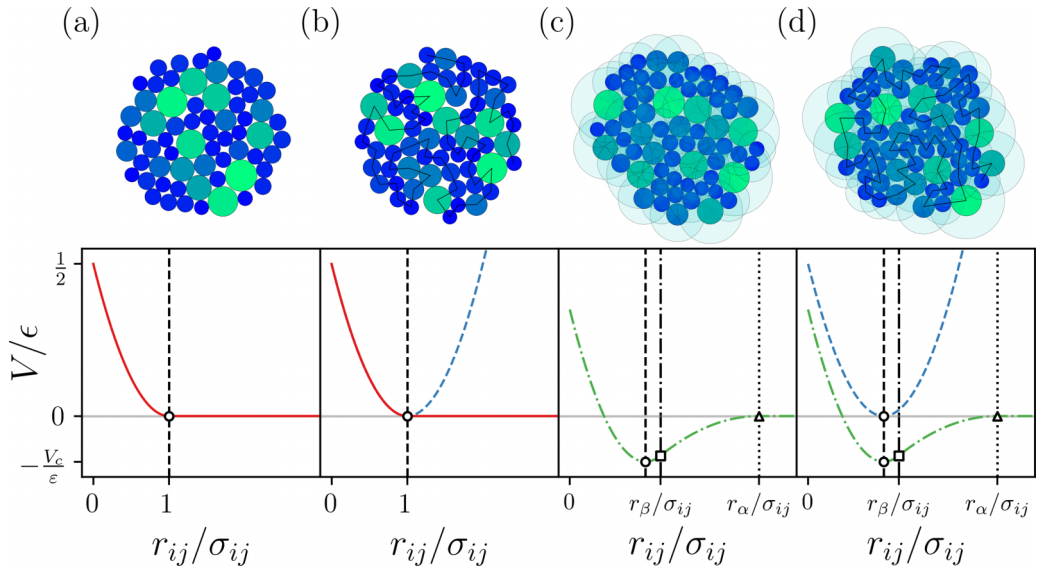

FIG. 1. Example static packings (above) and the corresponding potential energy V/ϵ (below) for (a) repulsive disk-shaped monomers, (b) repulsive polymers, (c) attractive disks, and (d) attractive polymers. The disk diameters are polydisperse, obeying an inverse power-law distribution for the diameters; the color shading indicates the particle size from large to small (light green to blue). The cyan shading in (c) and (d) indicates the range of the attractive interactions with $\alpha = 1.5$ [Eq. (3)]. The black solid lines connecting adjacent disks in (b) and (d) indicate the polymer backbone. The repulsive nonbonded interactions [Eq. (1)] is plotted as a red solid line, which is zero at contact (vertical dashed line and circle marker). The polymers include the same repulsive interactions and extend the interaction for $r_{ij} > \sigma_{ij}$ to a double-sided linear spring [Eq. (2)] for bonded disks (blue dashed line). Nonbonded attractive interactions are specified by an attractive range α and strength β [Eq. (3)] indicated by a green dot-dashed line. The nonbonded interaction is extended to $r_\beta/\sigma_{ij} = 1 + \sigma_{ij}\beta$ (vertical dot-dashed line and square marker where V changes concavity), after which V harmonically returns to zero at $r_\alpha/\sigma_{ij} = 1 + \alpha$ (vertical dotted line and triangle marker).

decreases [16,17]. To date, the only high-resolution experimentally determined protein cores that possess $\phi \gtrsim 0.55$ were solved using x-ray crystallography at extremely high pressures [18,19].

Numerous scattering experiments on protein structures have also suggested that, like glasses and jammed granular packings, proteins possess an excess of low-frequency modes in the vibrational density of states (VDOS) [20–23]. In the case of jammed repulsive disk packings, studies have established a connection between the form of the VDOS and isostaticity, where the number of interparticle contacts equals the number of degrees of freedom. Near jamming onset in these systems, the VDOS possesses a large excess, relative to the Debye prediction, of low-frequency, quasilocalized modes, which gives rise to anomalous mechanical properties [24–28].

Does the correspondence between the packing fraction of jammed packings of repulsive, disconnected amino-acid-shaped particles generated via rapid compression and the cores of experimentally determined proteins indicate a deep connection between the two systems or is it fortuitous? More generally, however, it is unknown what the connection is between polymer collapse and jamming onset, let alone for biological polymers such as proteins. To isolate the essential features of this more general problem, we can ask, for connected and disconnected spherical particles, what is the relationship between the thermal collapse of sticky, spherical bead-spring polymers or aggregation of sticky spherical particles and the onset of jamming of purely repulsive spherical particles under athermal, quasistatic compression?

Here, to understand the connection between the thermal collapse of sticky polymers and jamming of repulsive particles under athermal compression, we compare the interior packing fractions of static packings of single disk-shaped bead-spring polymers and static packings of disconnected disks, with either attractive or repulsive interactions in two dimensions, as shown in Fig. 1. For systems with nonbonded attractive interactions, we study the interior packing fraction as the system is cooled below the glass transition temperature at varying rates. For systems with purely repulsive nonbonded interactions, we develop an open-boundary "jamming" protocol where the system undergoes athermal, quasistatic compression until reaching a mechanically stable state using an externally applied radial force.

We find several important results. First, for a collapsed polymer with attractive nonbonded interactions to obtain interior packing fractions ϕ similar to those found for jammed packings of purely repulsive disks, they must be quenched well below the glass transition temperature. Additionally, we find that the attractive systems quenched to zero temperature and the repulsive systems compressed to jamming onset with open boundary conditions possess similar interior packing fractions for all system sizes, damping parameters, and initial temperatures studied for both disks and polymers. We show that packings of attractive disks and polymers possess excess low-frequency vibrational modes in the limit of small attractive strength. As expected, we find that repulsive disks compressed to jamming onset are isostatic. In contrast to prior work, we find that packings of repulsive polymers are hypostatic at jamming onset. However, the number of missing

contacts matches the number of "quartic" modes (i.e., the potential energy increases as δ^4 for displacements by δ along these modes), and thus packings of repulsive polymers are effectively isostatic. While packings of attractive monomers and polymers are hyperstatic when counting contacts using the full interaction potential, we find they can also be considered to be effectively isostatic if we appropriately redefine the interparticle contact network according to the attractive potential used. By varying the attractive strength, we observe the same scaling of the low-frequency modes of the vibrational density of states, $D(\omega)$, and excess number of contacts ΔN from the isostatic number versus the potential energy as found for repulsive disk packings compressed above jamming onset.

This article is organized into three additional sections and three Appendices. In Sec. II, we describe the numerical models for the disk-shaped bead-spring polymers and disk-shaped monomers with nonbonded attractive and repulsive interactions and the packing generation protocols. In Sec. III, we present the results for the interior packing fraction, characteristic plateau frequency of the vibrational density of states, $D(\omega)$, and contact number for each system. Finally, in Sec. IV, we discuss the implications of the results for understanding the dynamics of polymer collapse and protein folding and propose future work on jamming onset in all-atom protein models. In Appendix A we provide additional details on the packing-generation protocol. In Appendix B, we describe methods to avoid size segregation when applying a radial force to generate jammed packings of repulsive monomers and polymers in open boundary conditions. In Appendix C, we describe methods for identifying holes, or connected void space, in jammed packings.

II. NUMERICAL METHODS

A. Model systems

We study four types of systems: single disk-shaped bead-spring polymers with attractive nonbonded interactions, attractive disks (or monomers), single disk-shaped bead-spring polymers with repulsive nonbonded interactions, and repulsive disks (or monomers) as shown in Fig. 1. The nonbonded, repulsive interactions are modeled by the repulsive linear spring potential,

$$\frac{V^{\rm rnb}(r_{ij})}{\epsilon} = \frac{1}{2}\left(1-\frac{r_{ij}}{\sigma_{ij}}\right)^2\Theta\left(1-\frac{r_{ij}}{\sigma_{ij}}\right), \tag{1}$$

where r_{ij} is the center-to-center distance between disks i and j, σ_{ij} is their average diameter, ϵ is the energy scale of the repulsive interaction, and $\Theta(x)$ is the Heaviside step function. For the $N-1$ bonded interactions between disks i and $j=i+1$ in the bead-spring polymer, the repulsive linear spring potential is extended into a double-sided linear spring potential:

$$\frac{V^{b}(r_{ij})}{\epsilon} = \frac{1}{2}\left(1-\frac{r_{ij}}{\sigma_{ij}}\right)^2. \tag{2}$$

We parametrize the nonbonded attractive interactions by the attractive cutoff distance α and depth β. Previous work on jamming of spherical particles with short-ranged attractive interactions used a single parameter to characterize the attractive interactions [29–31]. Here we separate the attractive range and depth to allow the model to capture both short-ranged, sticky disks and molecular liquids with weak but long-range attractive interactions. For the nonbonded attractive interactions, we extend the potential in Eq. (1) to $r_\beta > \sigma_{ij}$ and cut off the interactions at $r_\alpha = (1+\alpha)\sigma_{ij} > r_\beta$:

$$\frac{V^{\rm anb}(r_{ij})}{\epsilon} = \begin{cases} \frac{1}{2}\left(1-\frac{r_{ij}}{\sigma_{ij}}\right)^2 - V_c/\epsilon & \text{for } r_{ij} \leqslant r_\beta \\ -\frac{k}{2\epsilon}\left(\frac{r_{ij}}{r_\alpha}-1\right)^2 & \text{for } r_\beta < r_{ij} \leqslant r_\alpha \\ 0 & \text{for } r_{ij} > r_\alpha \end{cases}, \tag{3}$$

where $V_c/\epsilon = (k/\epsilon)(r_\beta/r_\alpha - 1)^2/2 + (1-r_\beta/\sigma_{ij})^2/2$. The pair potential energy for repulsive disks is $V(r_{ij}) = V^{\rm rnb}(r_{ij})$ [Fig. 1(a)] and for repulsive polymers is $V(r_{ij}) = V^{b}(r_{ij}) + V^{\rm rnb}(r_{ij})$ [Fig. 1(b)]. For attractive disks $V(r_{ij}) = V^{\rm anb}(r_{ij})$ [Fig. 1(c)] and for attractive polymers $V(r_{ij}) = V^{b}(r_{ij}) + V^{\rm anb}(r_{ij})$ [Fig. 1(d)]. The total potential energy and interparticle forces for each system are given by $V = \sum_{i>j} V(r_{ij})$ and $\vec{F}_{ij} = -(dV/dr_{ij})\hat{r}_{ij}$. Note that we set $F_{ij}(r_\beta) = -\epsilon\beta/\sigma_{ij}$ and $k/\epsilon = (\beta r_\alpha/\sigma_{ij})(r_\beta/r_\alpha - 1)$ to ensure that the nonbonded energy and forces are continuous as shown in Fig. 1. Below we consider dimensionless forces $F_{ij}\sigma_s/\epsilon$, potential energies V/ϵ, frequencies $\sqrt{\epsilon/m}\sigma_s^{-1}$, and temperature k_bT/ϵ, where $k_b = 1$ is the Boltzmann constant, m is the mass of each disk, and σ_s is the size of the smallest disk.

To prevent crystallization [32] during the packing generation process, the disk diameters are selected randomly from a power-law size distribution, $P(\sigma_i) = A\sigma_i^{-3}$, where A is a normalization constant, σ_s and $\sigma_{\rm max} = 2.2\sigma_s$ are the minimum and maximum diameters, and the polydispersity $D = (\langle\sigma_i^2\rangle - \langle\sigma_i\rangle^2)/\langle\sigma_i\rangle^2 \sim 0.23$. For each system size of N disks, we average over 100 different sets of diameters $\{\sigma_i\}$ that were randomly selected from $P(\sigma_i)$.

B. Packing-generation protocol

For packing-generation protocols, the initial configurations influence the final jammed packings [24]. Therefore, in this study, we consider similar sets of initial configurations for all four systems: attractive and repulsive bead-spring polymers and attractive and repulsive disks. To achieve the initial states, we generate liquid globule configurations of attractive bead-spring polymers at initial temperatures $T_g < T_0 < T_m$, where the melting temperature T_m is defined as the midpoint of the radius of gyration versus temperature curve and the glass transition temperature T_g indicates the divergence of the structural relaxation time as a function of decreasing temperature, as discussed in Appendix A. The initial disk configurations can be obtained from the liquid globules by replacing the bonded interactions with nonbonded interactions and the purely repulsive configurations can be obtained from the liquid globules by replacing the nonbonded attractive interactions with purely repulsive interactions. Packings at jamming onset for all four systems can then be generated via damped molecular dynamics (MD) simulations at varying dissipation rates b using the appropriate potential energy functions, coupled with a thermal quenching schedule for systems with attractive interactions and a compression protocol with an applied radial force for systems with purely repulsive interactions. For additional

details concerning the packing-generation process for repulsive disks, repulsive polymers, attractive disks, and attractive polymers and the methods for identifying surface disks and calculating the core packing fraction, see Appendix A.

III. RESULTS

In this section, we describe the structural and mechanical properties of static packings of disks and disk-shaped bead-spring polymers with purely repulsive, as well as attractive interactions. In Sec. III A, we first show that when attractive disk-shaped bead-spring polymers are cooled toward the glass transition temperature T_g, the average packing fraction of the interior (or core region) is well below values given for random close packing for disordered packings of repulsive disks. Therefore, in Sec. III B we study the core packing fraction of attractive polymers as they are cooled from $T_0 > T_g$ to zero temperature using damped MD simulations. We find that attractive disk-shaped bead-spring polymers, as well as attractive disks, when cooled to zero temperature, possess similar core packing fractions as found for static packings of repulsive disks and disk-shaped bead-spring polymers over a wide range of initial temperatures T_0, damping parameters b, and system sizes N. In Sec. III C, we show that attractive disks and disk-shaped bead-spring polymers quenched to zero temperature possess an excess number of low-frequency modes in the VDOS (similarly to jammed packings of repulsive disks). We further show that slowly increasing the depth β of the attractive interparticle potential causes the attractive packings to lose low-frequency modes in a way that is similar to compression of repulsive disk packings above jamming onset. In Sec. III D, we find that, contrary to previous studies [33], static packings of repulsive disk-shaped bead-spring polymers are hypostatic at jamming onset, but the number of missing contacts relative to the isostatic number matches the number of "quartic" modes, such that the potential energy increases as δ^4 for displacements δ along these modes [34,35]. When we account for the quartic modes in packings of repulsive polymers, the excess number of contacts above isostaticity scales as $\Delta N \sim (V_r N^3)^\lambda$ as we found for packings of repulsive disks, where V_r is the total repulsive potential energy of the packing, $\lambda = 1/2$ at small ΔN, and the exponent crosses over to $\lambda = 1/4$ in the large-ΔN limit. Finally, in Sec. III E we show that packings of attractive disks and of disk-shaped bead-spring polymers are also effectively isostatic if contacts are defined as $r_{ij} < r_\beta$ and they obey the same scaling of the excess number of contacts with the repulsive energy, $\Delta N \sim (V_r N^3)^\lambda$, as found for static packings of repulsive disks and disk-shaped bead-spring polymers.

A. Core packing fraction for collapsed polymers near T_g is well below random close packing for repulsive disks

What is the core packing fraction of an attractive disk-shaped bead-spring polymer as it is cooled toward the glass transition temperature T_g? (For a discussion of estimates of the melting temperature T_m and T_g in attractive systems, see Appendix A.) In Fig. 2, we plot the average core packing fraction $\langle\phi\rangle$ versus $T - T_g$ for $N = 256$ averaged over 100 attractive polymers with different initial conditions. The core packing fraction increases with decreasing temperature, $\langle\phi\rangle_g - \langle\phi\rangle \sim (T - T_g)^\gamma$, approaching the plateau value of $\langle\phi\rangle_g \approx 0.796$ as $T \to T_g$ (with $\gamma \approx 0.9$). $\langle\phi\rangle_g$ is similar to values reported for the packing fraction near the glass transition in experimental, computational, and theoretical studies of hard spheres in two dimensions [36,37]. In contrast, static packings of $N = 256$ purely repulsive polydisperse disks, without a polymer backbone, possess a much larger packing fraction, $\langle\phi\rangle \approx 0.835$, at jamming onset [24]. The core packing fraction for collapsed attractive polymers near T_g is far below that for static packings of purely repulsive disks at jamming onset. This result indicates that for the core packing fraction of collapsed attractive polymers to reach those of jammed disconnected, repulsive disks, they must be cooled to temperatures much below the glass transition temperature.

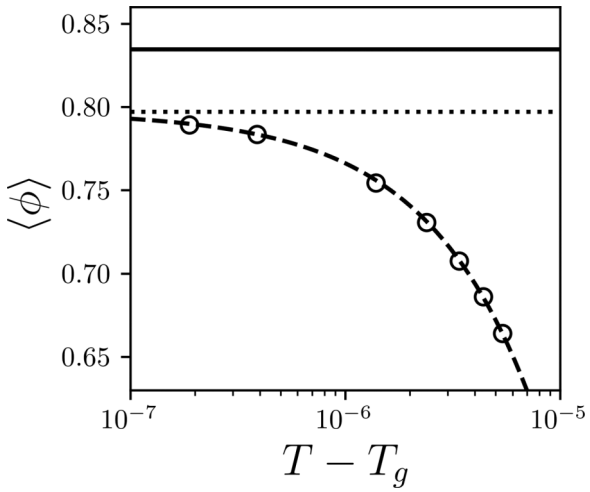

FIG. 2. The average core packing fraction $\langle\phi\rangle$ is plotted versus $T - T_g$. The dashed line gives $\langle\phi\rangle_g - \langle\phi\rangle \sim (T - T_g)^\gamma$, where $\langle\phi\rangle_g \approx 0.796$ (dotted line) and $\gamma \approx 0.9$. The horizontal solid line at $\langle\phi\rangle \approx 0.835$ indicates the average packing fraction at jamming onset for repulsive monomers under periodic boundary conditions.

B. Core packing fraction for collapsed polymers with $T \ll T_g$ matches that for jammed repulsive packings

To study the core packing fraction of collapsed, attractive polymers below the glass transition temperature T_g, we performed damped MD simulations to take attractive polymers with initial temperatures $T_m > T_0 > T_g$ to zero temperature using a wide range of damping parameters. In Fig. 3, we show that the core packing fraction of collapsed, attractive polymers increases with decreasing damping parameter from roughly 0.83 to 0.85 (circles with solid lines) for $N = 512$. For high damping parameters, higher initial temperatures T_0 give rise to the lowest values of the core packing fraction. However, for low damping parameters, the results for the core packing fraction of collapsed, attractive polymers are the same for all T_0. To study the effects of the polymer backbone constraint on the core packing fraction, we repeat these simulations for disconnected, attractive disks (squares with solid lines). The dependence of $\langle\phi\rangle$ on the damping parameter b and initial temperature T_0 is similar to that for collapsed, attractive

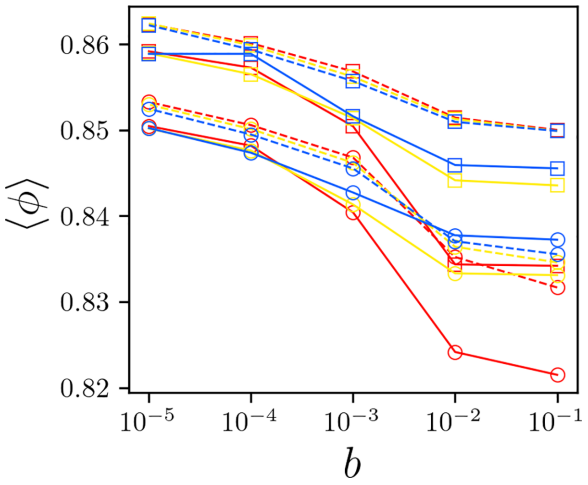

FIG. 3. The average core packing fraction $\langle\phi\rangle$ from damped MD simulations plotted versus the damping parameter b for attractive disk-shaped bead-spring polymers (circles with solid lines), attractive disks (squares with solid lines), repulsive disk-shaped bead-spring polymers (circles with dashed lines), and repulsive disks (squares with dashed lines), prepared from initial temperatures $T_0/T_m = 0.43$ (red), 0.32 (yellow), and 0.27 (blue) for $N = 512$.

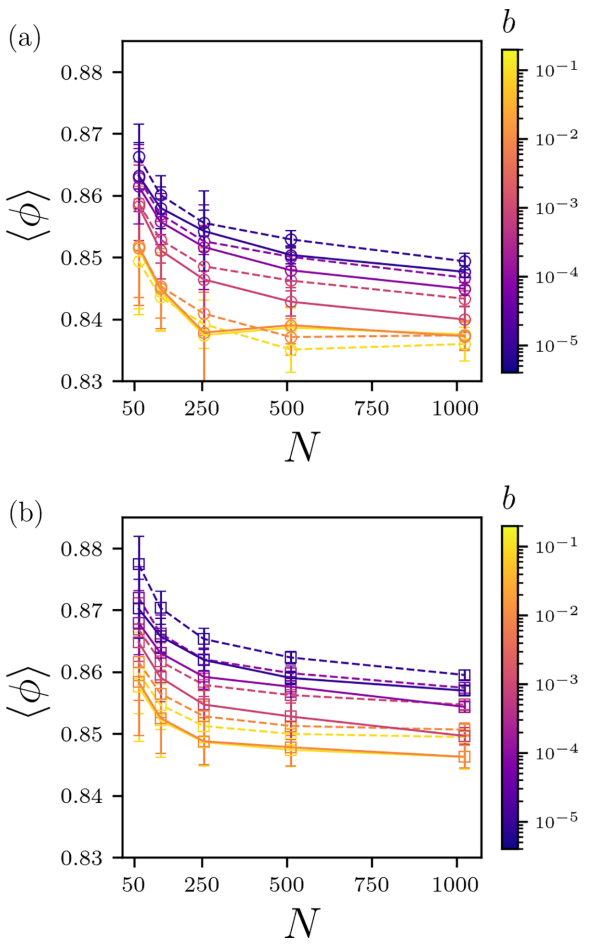

FIG. 4. The core packing fraction $\langle\phi\rangle$ from damped MD simulations averaged over all initial temperatures T_0 and plotted versus the system size N and damping parameter b (increasing from purple to yellow). We show results for (a) collapsed, attractive polymers (circles with solid lines) and jammed repulsive polymers (circles with dashed lines) and (b) attractive disks (squares with solid lines) and jammed repulsive disks (squares with dashed lines). Void regions are identified using probe size $\sigma_p/\sigma_s = 1$ and core disks adjacent to void regions are not included in the calculation of $\langle\phi\rangle$.

polymers; however, the packing fraction is shifted to larger values by ≈0.01 for all b and T_0.

To compare the core packing fraction of collapsed, attractive polymers to the packing fraction of jammed repulsive systems, we developed a novel compression protocol to generate jammed repulsive systems in open boundary conditions. (See Appendix B.) We start with the same attractive polymer configurations prepared at T_0 for both polymers and disconnected disks. We then replace the nonbonded attractive interactions ($V^{\rm anb}$) with nonbonded repulsive interactions ($V^{\rm rnb}$) and compress the system isotropically by attaching each disk to a radial linear spring anchored to the origin. In Fig. 3, we show the core packing fraction for jammed packings of repulsive disk-shaped bead-spring polymers (circles with dashed lines) and repulsive disks (squares with dashed lines). For these purely repulsive systems, the core packing fraction does not depend strongly on T_0. Further, for small T_0, the collapsed, attractive polymers and jammed repulsive polymers possess similar core packing fractions for all damping parameters b. In addition, there is qualitative agreement for the core packing fraction of packings of disconnected attractive and repulsive disks for all b. These results emphasize that the attractive interactions do not strongly influence the core packing fraction, i.e., structures that collapse due to attractive interactions are similar to those that form due to mechanical compression with weak thermal fluctuations.

As discussed above, the core packing fraction for collapsed, attractive polymers is the lowest for high damping parameters b and high initial temperatures T_0. We find that these collapsed structures possess large void regions surrounded by regions that are densely packed. See Appendix C for details on how we identify disks that occur near interior void regions. When we do not consider disks that are adjacent to void regions, the core packing fraction results converge for different initial temperatures. Thus, aside from void regions, the initial temperature has only a minor effect on the packing fraction of dense core regions of collapsed, attractive polymers.

In Fig. 4, we present the results for the core packing fraction (averaged over all T_0 and excluding void regions) plotted versus the system size N and damping parameter b for [Fig. 4(a)] disk-shaped bead-spring polymers and [Fig. 4(b)] disconnected disks. In general, when we do not consider void regions, the core packing fraction for collapsed, attractive polymers matches that for jammed, repulsive polymers and the core packing fraction for packings of attractive disks matches that for jammed repulsive disks for all b and N. These results suggest that the structural properties of systems with attractive interactions that are cooled to zero temperature are similar to those for repulsive systems that are compressed to jamming onset. In addition, we find that the average core packing fraction *decreases* with increasing system size N, whereas packing-generation protocols that start from

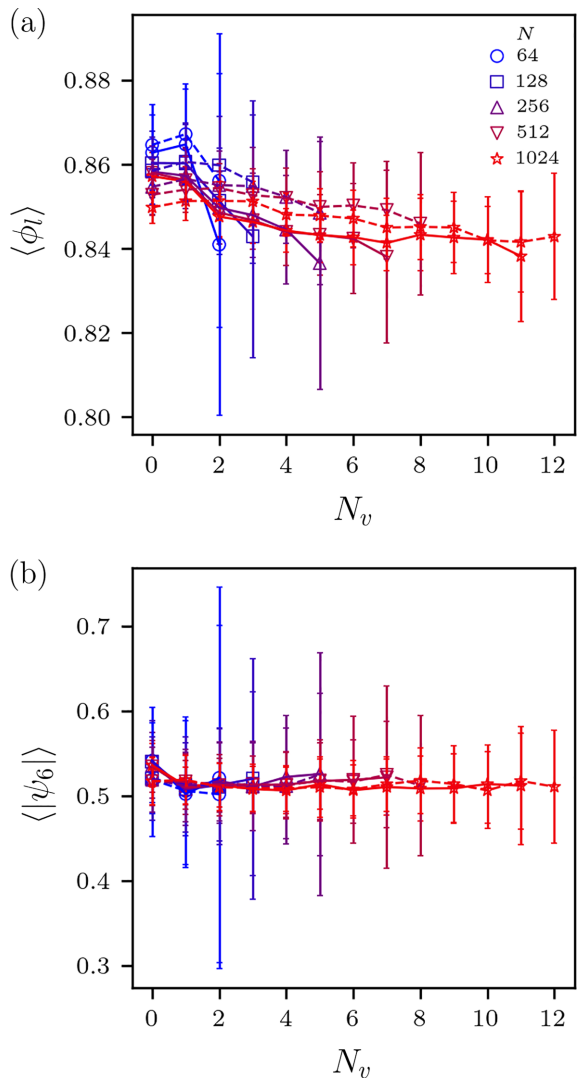

FIG. 5. (a) The local packing fraction $\langle\phi_l\rangle$ and (b) hexatic order parameter $\langle|\psi_6|\rangle$ for each disk plotted versus the number of Voronoi cells N_v between each disk and the closest surface disk for collapsed, attractive polymers (solid lines) and jammed, repulsive polymers (dashed lines) for several system sizes, $N = 64$ (circles), 128 (squares), 256 (upward triangles), 512 (downward triangles), and 1024 (stars) colored from blue to red with increasing system size N.

low-density configurations yield $\langle\phi\rangle$ that typically *increase* with N [24]. Note that jammed polymer packings possess slightly lower packing fractions than jammed disk packings. For polymers, $\langle\phi\rangle$ varies between 0.84 and 0.85 in the large-N limit. For disks, $\langle\phi\rangle \approx 0.85$–$0.86$ for large N.

To better understand the system-size dependence of $\langle\phi\rangle$, we also calculate the local core packing fraction ϕ_l as a function of the distance to the surface of the packing. For small packings, a relatively large fraction of the disks are located near the curved boundaries. As N increases, a larger number of disks are considered bulk, far from the curved boundaries. In Fig. 5(a), we plot the local core packing fraction ϕ_l versus the number of Voronoi cells N_v between a given disk and the closest surface disk for collapsed, attractive polymers and jammed, repulsive polymers. ($N_v = 0$ indicates that a core disk is adjacent to a surface disk.) We find that the core packing fraction for both attractive and repulsive polymers is largest for small systems and near surface disks. As N_v increases, $\langle\phi_l\rangle$ decreases and converges in the large-system limit. In addition, $\langle\phi_l\rangle$ is more uniform for jammed, repulsive polymer packings than for attractive polymers, indicating a surface tension effect on the packing of attractive polymers.

We also calculated the local hexatic order parameter associated with each core disk,

$$|\psi_6| = \frac{1}{n_k}\left|\sum_{j=1}^{n_k} e^{6i\theta_{jk}}\right|, \tag{4}$$

where θ_{jk} is the angle between a central core disk k and its Voronoi neighbors $j = 1, \ldots, n_k$, to determine whether increases in the core packing fraction are correlated with increases in positional order. In Fig. 5(b), we show that $\langle|\psi_6|\rangle \sim 0.5$ is independent of N_v and comparable to values for amorphous jammed disk packings [38].

C. Low-frequency contribution to the density of vibrational modes

Above, we showed that the core packing fractions for collapsed, attractive polymers and packings of attractive disks are similar to those of jammed repulsive polymers and repulsive disks. Do these disparate systems also share other structural and mechanical properties of jammed packings of repulsive disks? We first consider the VDOS $D(\omega)$, which is obtained by calculating the dynamical matrix,

$$M_{kl} = \frac{\partial^2 V}{\partial\vec{r}_k\partial\vec{r}_l}, \tag{5}$$

where k and l label the $2N$ coordinates of the disks. The eigenvectors $\vec{\xi}_k^i = \{e_{1x}^i, e_{1y}^i, \ldots, e_{Nx}^i, e_{Ny}^i\}$ represent an orthogonal set of $2N$ normal modes whose eigenvalues e^i correspond to the normal mode frequencies $\omega^i = \sqrt{e^i}$. $D(\omega)$ does not depend strongly on the initial temperature T_0 or the damping parameter b used to generate the packings, and we focus on packings prepared using $T_0/T_m = 0.27$ and $b = 10^{-5}$. To generate mechanically stable repulsive packings, we jammed the repulsive disks and polymers under circular boundary conditions. Specifically, we initialize the repulsive packings analyzed in Sec. III B and then apply sequential affine compressions of $\Delta\phi = 10^{-3}$ followed by overdamped energy minimization until reaching a target potential energy $V_r/N = 10^{-14}$, where $V_r = V^{\rm rnb} + V^w$ for repulsive disks and $V_r = V^{\rm rnb} + V^b + V^w$ for repulsive polymers. Additionally, underconstrained disks associated with zero-modes are removed—rattlers in the case of repulsive disks and flippers in the case of repulsive polymers. (See Sec. III D for further details.) In Figs. 6(a) and 6(b), we show the density of vibrational states $D(\omega)$ for packings of repulsive disks and packings of repulsive polymers, respectively. As expected, $D(\omega)$ for jammed packings of repulsive disks possess an anomalous plateau at low frequencies rather than Debye behavior [24]. Similarly, packings of repulsive polymers also display a low-frequency plateau over the range $10^{-2} < \omega < 10^{-1}$ in Fig. 6(b). However, there are further excess vibrational modes in packings of repulsive polymers for $\omega < 10^{-2}$, which

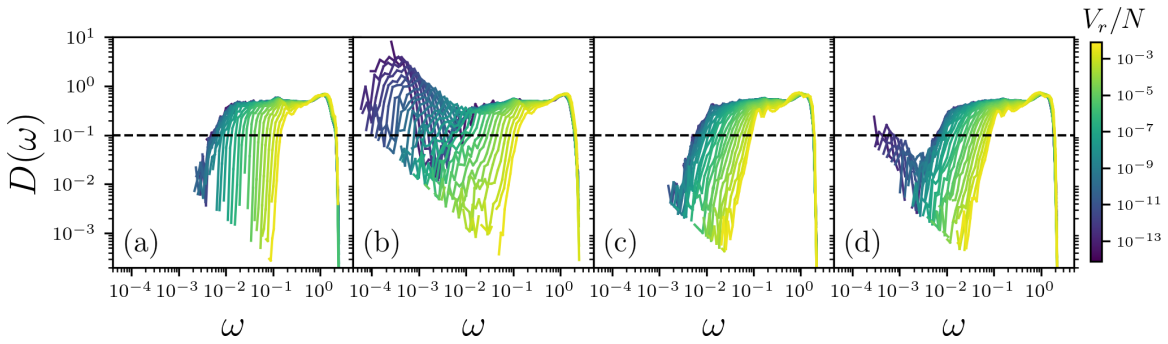

FIG. 6. The vibrational density of states $D(\omega)$ for jammed packings of (a) repulsive disks, (b) repulsive polymers, (c) attractive disks, and (d) attractive polymers, colored by V_r/N (increasing from purple to yellow) for $N = 128$. The black dashed line defines the characteristic frequency ω^*, where $D(\omega^*) = 10^{-1}$. Note the large low-frequency peak for packings of repulsive and attractive polymers in (b) and (d), which arise due to quartic modes. Quartic modes are removed from $D(\omega)$ when calculating ω^*. (See Sec. III D.)

indicate the presence of quartic modes that are discussed below in Sec. III D.

When the attractive interactions are weak, i.e., $\beta = 10^{-5}$ as discussed in Sec. III B, attractive disk and polymer packings possess only small disk overlaps, $V_r/N \lesssim 10^{-14}$, where $V_r = V^{\rm rnb}$ for attractive disks and $V_r = V^{nrb} + V^b$ for attractive polymers. We find that $D(\omega)$ for attractive disk and attractive polymer packings with $V_r/N \lesssim 10^{-14}$ possess no nontrivial zero modes and a broad low-frequency plateau, similar to that obtained for jammed, repulsive disk packings prepared with comparable values of V_r as shown in Figs. 6(c) and 6(d). The small peak at the lowest frequencies in packings of attractive polymers indicates the presence of quartic modes.

When we compress repulsive disk and polymer packings above jamming onset by increasing ϕ and thus V_r (from purple to yellow), the plateau in $D(\omega)$ at low frequencies decreases, as shown in Figs. 6(a) and 6(b) [25,26]. Effective compression of attractive packings can be obtained by increasing the attractive depth β. In Figs. 6(c) and 6(d), we vary the attractive depth by successively multiplying β by a factor of $r \sim 1.12$ in the range $10^{-8} < \beta < 10^{-1}$ followed by overdamped energy minimization after each change in β. Increasing β gives rise to concomitant increases in V_r and a loss of the low-frequency plateau.

We quantify the anomalous low-frequency plateau in $D(\omega)$ by identifying a characteristic frequency ω^* at which $D(\omega^*)$ falls below a small threshold. Here we use $D(\omega^*) = 10^{-1}$, but the results are similar over a range of thresholds. In Fig. 7(a), we show ω^* as a function of V_r for packings of repulsive disks compressed under circular boundary conditions for several system sizes $N = 64$, 128, 256, 512, and 1024. Previous work has shown that under periodic boundary conditions the characteristic plateau frequency scales as $\omega^* N \sim (PN^2)^{1/2}$ at high pressures P [25,26,28]. Attractive packings with no boundaries are at zero pressure, and thus we plot their low frequency response against V_r instead of P. Potential energy V and pressure P in repulsive systems have a known scaling relation of $P \sim (V/N)^{1/2}$ [24]. Combining these two scaling relations gives $\omega^* N \sim (VN^3)^{1/4}$, which is plotted as black dashed line in Fig. 7(a) [39]. Additionally, we show in Fig. 7(b) that compressing repulsive polymer packings above jamming onset gives nearly identical results for $\omega^* N$ versus $V_r N^3$ as found for repulsive disk packings, when quartic modes are removed. This result indicates, at least in the harmonic approximation, double-sided polymer bonds do not strongly affect the low-frequency mechanical response.

Does the power-law scaling of ω^* versus V_r still hold for attractive packings as we increase β and thus V_r? In Figs. 7(c) and 7(d), we show that increasing the attraction depth is similar to overcompression of a repulsive disk packing, i.e., both lead to a decrease in the low-frequency plateau in $D(\omega)$ and give rise to $\omega^* N \sim (V_r N^3)^{1/4}$ for the finite-size scaling of the plateau frequency. In Fig. 7, we achieved an effective compression of attractive packings by increasing the attractive depth β, while fixing the attractive interaction range at $\alpha = 1.5$. In Sec. III E we address varying α as well as β and find similar results.

D. Repulsive polymer packings are hypostatic but effectively isostatic

Jammed packings of repulsive disks are known to be isostatic, i.e., the onset of rigidity occurs when the number of constraints (arising from interparticle and particle-wall contacts) equals the number of degrees of freedom, which controls the vibrational and mechanical response of jammed packings [24,27,28]. For isostatic packings, the number of contacts at jamming onset satisfies: $N_c^{\rm iso} = 2(N - N_r) + f(d) + 1$, where N_r is the number of underconstrained rattler particles, $f(d)$ indicates the number of unconstrained degrees of freedom from the boundary conditions [e.g., $f(d) = 1$ for circular fixed boundaries in $d = 2$], and the $+1$ corresponds to the particle size degree of freedom [24,40]. Rattler particles for packings of repulsive disks correspond to particles with fewer than three contacts or particles where all contacts occur on a semicircle. Rattler particles are identified and removed iteratively. Previous studies have shown that compressing jammed packings gives rise to an increase in interparticle contacts, which in turn increases the characteristic plateau frequency ω^* [25,26]. In Fig. 8(a), we plot $\Delta N = N_c + N_w - N_c^{\rm iso}$ versus $V_r N^3$, where N_c is the number of interparticle contacts and N_w is the number of particle-wall contacts. We show that ΔN obeys power-law scaling with V_r/N: $\Delta N \sim (V_r N^3)^{\lambda}$, where $\lambda = 1/2$ for $V_r N^3 \lesssim 1$ and $\lambda = 1/4$ for $V_r N^3 \gtrsim 1$. These results match those for the finite-size scaling of the pressure dependence of ΔN and shear

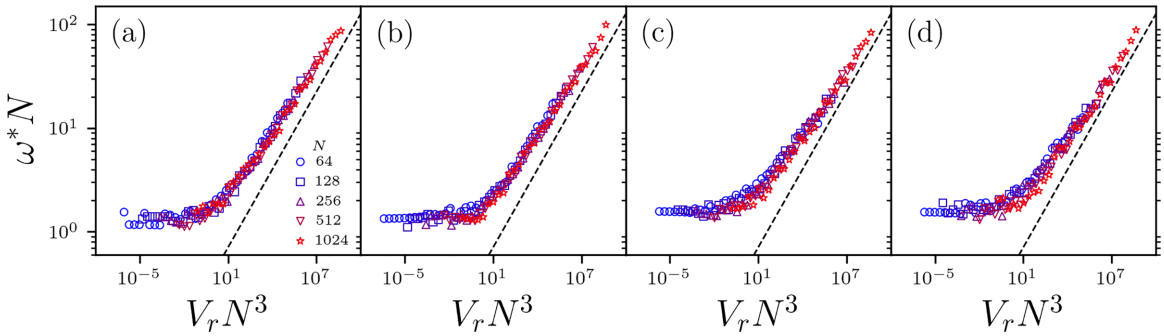

FIG. 7. Characteristic plateau frequency of the vibrational density of states $\omega^* N$ versus potential energy $V_r N^3$ for jammed packings of (a) repulsive disks, (b) repulsive polymers, (c) attractive disks, and (d) attractive polymers for several system sizes, $N = 64$ (circles), 128 (squares), 256 (upward triangles), 512 (downward triangles), and 1024 (stars) colored from blue to red with increasing system size. The dashed line has a slope of 1/4.

modulus G for jammed packings of repulsive disks and spheres [28,41], i.e., $\Delta N \sim G \sim (PN^2)^\mu$, where $\mu = 1$ for $PN^2 \lesssim 1$ and $\mu = 1/2$ for $PN^2 \gtrsim 1$.

Previous studies have suggested that jammed packings of repulsive polymers are isostatic [33,42]. However, one must carefully identify "flipper" particles that have too few contacts to be fully constrained, as well as quartic modes. We find that jammed packings of repulsive polymers are in fact *hypostatic* but are effectively isostatic when accounting for flippers and quartic modes. Previous work identified flipper particles as those with no nonbonded interactions [33,43]. Here we use (nonrotational) zero modes of the dynamical matrix $\vec{\xi}^i$ to identify underconstrained flipper particles in repulsive polymer packings. We successively remove the largest contribution $\{e^i_{jx}, e^i_{jy}\}$ to $\vec{\xi}^i$ until it is no longer a zero mode. Each particle j with the largest contribution to the zero mode is identified as a flipper particle. In Fig. 9(a), the yellow-shaded particles are flippers since they only have bonded contacts, one of their neighbors only has bonded contacts, and they can collectively rotate without changing the length of the bonds and without making additional contacts. The red and cyan particles have no nonbonded contacts, but their bonded neighbors have at least one nonbonded contact, and so they are not flipper particles.

The red arrows in Fig. 9(a) indicate a quartic mode in a repulsive polymer packing. The cyan particle has the largest contribution to the quartic mode and its motion is perpendicular to the approximately 180° bond angle. When we perturb a packing by an amplitude δ along a typical eigenvector $\vec{\xi}^i$ of the dynamical matrix, the change in potential energy $\Delta V \sim \delta^2$ scales quadratically with the amplitude as shown in Fig. 9(b) where $V = V^{\rm rnb} + V^b + V^w$. However, hypostatic packings contain quartic modes, such that the change in energy ΔV for perturbations with amplitude δ along a quartic mode scale as $\Delta V \sim \delta^4$ [35]. In Fig. 9(b), we show the quartic scaling for $\delta \gtrsim \delta_q$, where $\delta_q \sim P$ varies linearly with pressure, for perturbations along the quartic mode given in Fig. 9(a).

Since the change in potential energy for perturbations along quartic modes scales quadratically with the amplitude of the perturbation for $\delta \lesssim \delta_q$, it can be challenging to identify quartic modes. To count the number of quartic modes, we decompose the dynamical matrix into two components, the stiffness matrix H and stress matrix S, where $M = H + S$ [34,35]. The stiffness matrix only depends on the geometry of the system (not the interaction potential or pressure),

$$H_{kl} = \sum_{i>j} \frac{\partial^2 V}{\partial(\vec{r}_{ij}/\sigma_{ij})^2} \frac{\partial(r_{ij}/\sigma_{ij})}{\partial \vec{r}_k} \frac{\partial(r_{ij}/\sigma_{ij})}{\partial \vec{r}_l}, \tag{6}$$

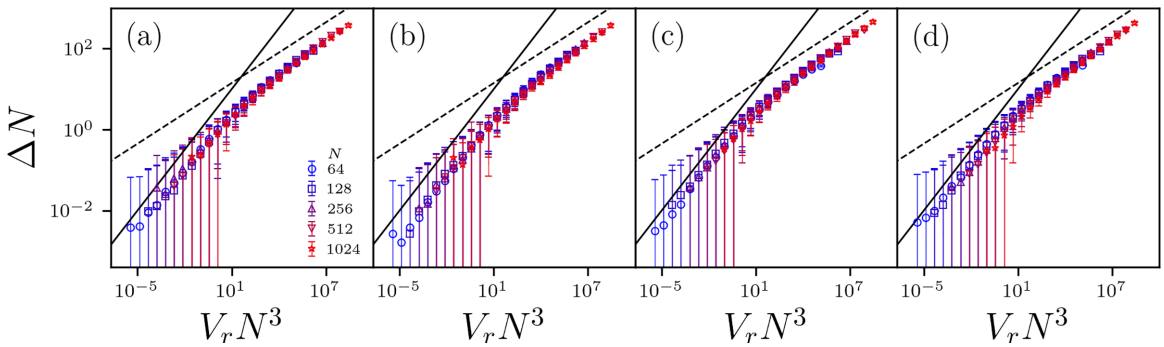

FIG. 8. Excess contact number above isostaticity $\Delta N = N_c' - N_c^{\rm iso}$ versus potential energy $V_r N^3$ for packings of (a) repulsive disks ($N_c' = N_c + N_w$), (b) repulsive polymers ($N_c' = N_c + N_w + N_b + N_q$), (c) attractive disks [$N_c' = N_c(r_{ij} < r_\beta) + N_b$], and (d) attractive polymers [$N_c' = N_c(r_{ij} < r_\beta) + N_b + N_q$] as a function of system size, $N = 64$ (circles), 128 (squares), 256 (upward triangles), 512 (downward triangles), and 1024 (stars) colored from blue to red with increasing system size. N_c is the number of interparticle contacts, N_w is the number of particle-wall contacts, N_b is the number of polymer bonds, and N_q is the number of quartic modes. The solid line indicates slope 1/2 and the dashed line indicates slope 1/4. Error bars indicate one standard deviation in ΔN.

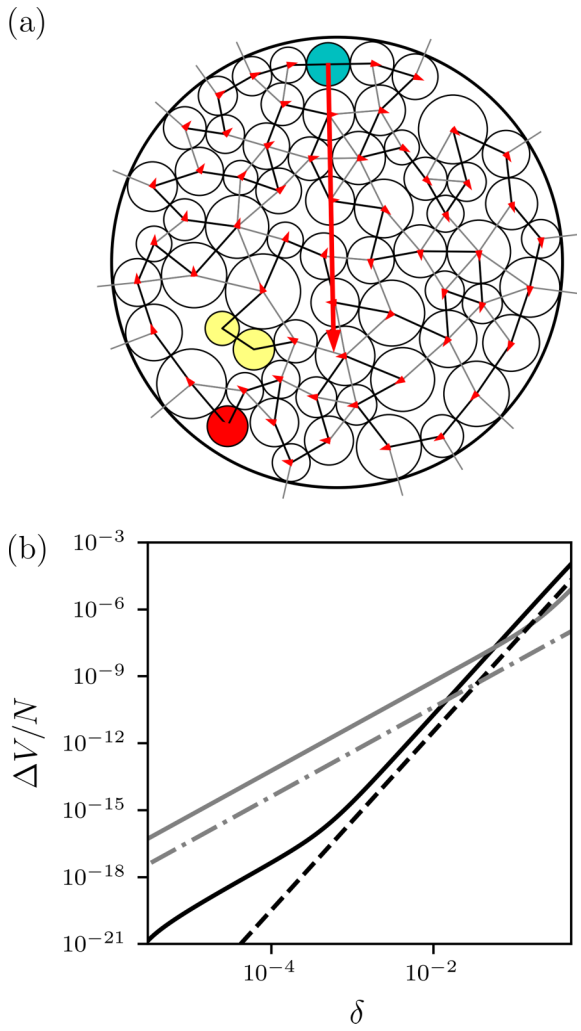

FIG. 9. (a) Jammed repulsive polymer packing showing the quartic mode in (b) with red arrows for $N = 64$. Gray lines indicate interparticle and particle-wall contacts. Black lines indicate the polymer backbone. The large black circle that encloses the polymer indicates the circular wall. Nonflipper disks are colored white. The pair of yellow disks are underconstrained flippers. The cyan disk has no nonbonded contacts and participates most directly in the quartic mode. The red disk also has no nonbonded contacts but does not lead to a quartic mode. (b) Change in potential energy $\Delta V/N$ following a perturbation with amplitude δ applied along an eigenvector of the dynamical matrix for a jammed repulsive polymer packing corresponding to a quadratic (gray solid line) and quartic mode (black solid line). Gray dot-dashed and black dashed lines indicate slopes of 2 and 4.

where k and l loop over all N particle coordinates. Previous work has shown that quartic modes $\vec{\xi}^i$ in M have nonzero eigenvalues e^i at nonzero pressure; however, the same eigenmode yields $H\vec{\xi}^i = h^i\vec{\xi}^i$, where $h^i = 0$ [35]. Therefore, for each repulsive polymer packing, we calculate the number of quartic modes $N_q = H_0 - M_0$, where M_0 and H_0 are the number of zero modes in the dynamical matrix and stiffness matrix, respectively. We find that packings of repulsive polymers are hypostatic at jamming onset with $N_c + N_w + N_b < N_c^{\rm iso}$, where N_b is the number of polymer bonds. However, the number of missing contacts $N_m = N_c^{\rm iso} - N_c - N_w - N_b$ equals the number of quartic modes $N_m = N_q$ for each repulsive polymer packing. As shown Fig. 8(b), we find identical finite-size scaling and collapse of the excess number of contacts ΔN versus $V_r N^3$ for packings of repulsive polymers and packings of repulsive disks, where $\Delta N = N_c + N_w + N_b + N_q - N_c^{\rm iso}$ for packings of repulsive polymers.

E. Attractive disk and polymer packings are hyperstatic but effectively isostatic

Above, we showed that repulsive packings are isostatic at jamming onset and obey power-law scaling relations for ω^* and ΔN versus $V_r N^3$. In addition, we find that attractive monomer and polymer packings not only possess similar core packing fractions as their repulsive counterparts, but also follow the same power-law scaling relation for ω^* versus $V_r N^3$. Can attractive disk and polymer packings be viewed as effectively isostatic as well?

Typical contact counting analyses consider a constraint as the onset of any nonzero interaction between particles or between a particle and a wall. Thus, for attractive systems in Eq. (3), a contact could be defined as an interparticle separation that satisfies $r_{ij}/\sigma_{ij} < 1 + \alpha$. With this definition, packings of attractive monomers and polymers are highly hyperstatic containing many more interactions than degrees of freedom. However, previous studies have suggested that weak long-range attractions are relatively unimportant for determining the mechanical properties of attractive solids [44]. Remarkably, using the attractive potential in Eq. (3), we find that if we count contacts as those with interparticle separations with $r_{ij}/r_\beta < 1$, packings of attractive monomers are effectively isostatic for small V_r, i.e., $N_c(r_{ij} < r_\beta) = N_c^{\rm iso}$, where $N_c^{\rm iso} = 2N - f(d)$ and $f(d) = 3$ for the two uniform translations and a single rotation that have no energy cost for attractive packings with open boundary conditions. In Eq. (3), r_β indicates a change in the interaction stiffness. For $r_{ij}/\sigma_{ij} < r_\beta$, $|\partial^2 V/\partial r_{ij}^2| \sim \epsilon$, whereas $|\partial^2 V/\partial r_{ij}^2| \sim k/\epsilon \sim \beta$ tends to zero as $\beta \to 0$ for $r_\beta < r_{ij} < r_\alpha$. In Fig. 8(c), we show that $\Delta N = N_c(r_{ij} < r_\beta) - N_c^{\rm iso}$ for attractive disks obeys the same power-law scaling with $V_r N^3$ as found for packings of repulsive disks and polymers.

We have shown that if we define contacts for packings of attractive disks as those with $r_{ij} < r_\beta$, attractive disk packings are effectively isostatic (for $V_r N^3 \ll 1$) and ΔN versus $V_r N^3$ obeys similar power-law scaling as that found for isostatic repulsive packings. However, do attractive packings with contacts defined by $r_{ij} < r_\beta$ possess any zero-energy modes? To address this question, we construct the stiffness matrix from contacts defined by $r_{ij}/r_\beta < 1$ in attractive disk packings. We then calculate the stiffness matrix eigenvalues $h^i(r_{ij} < r_\beta)$ and compare them to the eigenvalues of the stiffness matrix $h^i(r_{ij} < r_\alpha)$ using contacts defined by the full attractive potential. We not only find that attractive disk packings with contact networks defined by $r_{ij} < r_\beta$ are effectively isostatic, but also that $H(r_{ij} < r_\beta)$ has no nontrivial zero-energy modes, $h^i(r_{ij} < r_\beta) > 0$. We further show in Fig. 10(a) that for the attractive disks the eigenvalues $h^i(r_{ij} < r_\beta)$ are nearly identical to the eigenvalues $h^i(r_{ij} < r_\alpha)$.

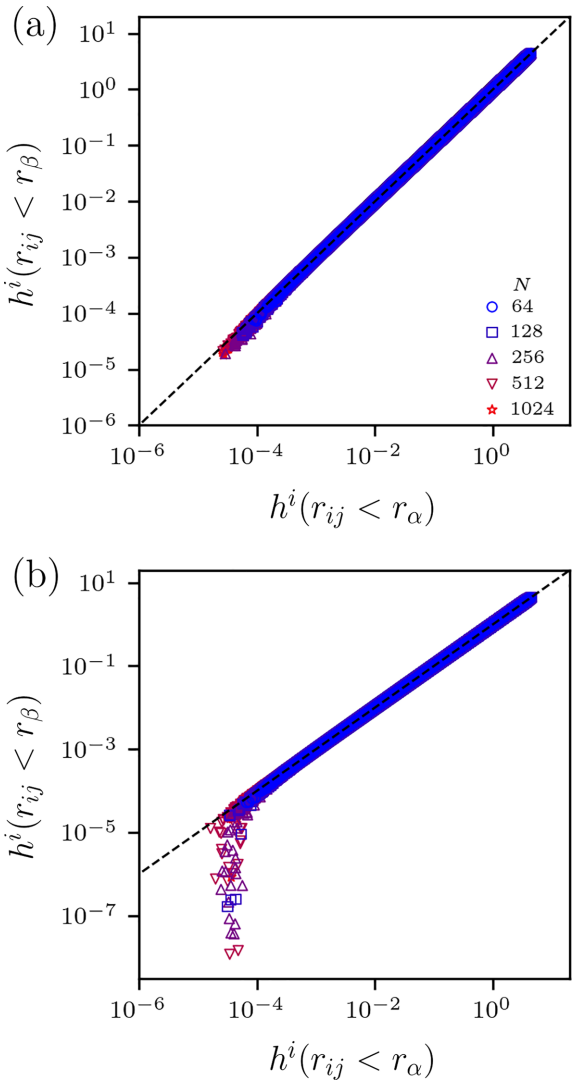

FIG. 10. The eigenvalues $h^i(r_{ij} < r_\beta)$ of the stiffness matrix $H(r_{ij} < r_\beta)$ for attractive packings with contacts defined by $r_{ij} < r_\beta$ plotted versus the eigenvalues $h^i(r_{ij} < r_\alpha)$ for $H(r_{ij} < r_\alpha)$ with contacts defined using the full attractive potential for attractive (a) disks and (b) polymers as a function of system size, $N = 64$ (circles), 128 (squares), 256 (upward triangles), 512 (downward triangles), and 1024 (stars) colored from blue to red with increasing system size. The black dashed line indicates $h^i(r_{ij} < r_\beta) = h^i(r_{ij} < r_\alpha)$.

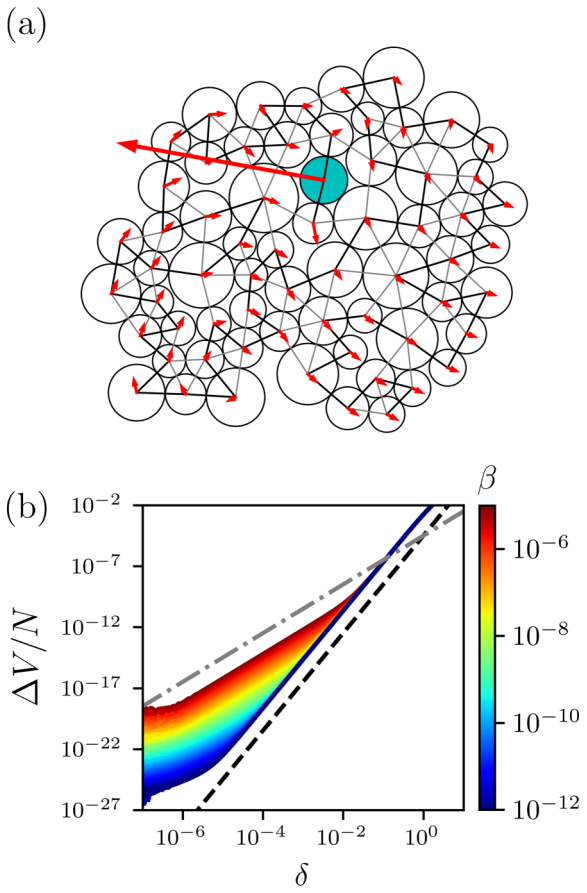

FIG. 11. (a) Illustration of an attractive polymer packing with $N = 64$ and $\beta = 10^{-5}$. We highlight the quartic mode in (b) with red arrows. The gray lines indicate contacts that satisfy $r_{ij} < r_\beta$ and the black lines indicate the polymer backbone. $N_c(r_{ij} < r_\beta) + N_b = 124$ and $N_c^{\rm iso} = 2N - 3 = 125$ and therefore the packing is missing a single contact. The cyan-shaded particle has no nonbonded contacts with $r_{ij} < r_\beta$ and has the largest contribution to the quartic mode. (b) Change in the total potential energy $\Delta V/N$ following a perturbation with amplitude δ applied along the quartic mode of the dynamical matrix in (a) for increasing attractive strength β (curves shaded from blue to red). The gray dot-dashed and black dashed lines indicate slopes of 2 and 4.

Are packings of attractive polymers effectively isostatic using the same definition of interparticle contacts as packings of attractive disks? When defining contacts as $r_{ij}/r_\beta < 1$, some attractive polymer packings appear to be hypostatic with $N_c(r_{ij} < r_\beta) + N_b < N_c^{\rm iso}$. For example, in Fig. 11(a), we show an attractive polymer packing with $N_c(r_{ij} < r_\beta) + N_b = 124$ and $N_c^{\rm iso} = 2N - 3 = 125$ and therefore this packing is missing a single contact. We find that the lowest nontrivial eigenmode of the dynamical matrix M is very similar to a quartic mode in a jammed repulsive polymer packing, where the largest contribution to the mode is perpendicular to an approximately 180° bond angle. For repulsive polymer packings, the number of quartic modes satisfies $N_q = H_0 - M_0$. In attractive polymer packings with missing contacts, $H_0 = M_0$ and N_q appears to be 0. However, we show in Fig. 11(b) that when we perturb the attractive polymer packing in Fig. 11(a) along the possible quartic mode of M, the change in the potential energy $V = V^{\rm anb} + V^b$ versus the perturbation amplitude δ scales as $\Delta V_r \sim \delta^4$ for $\delta > \delta_q \sim \beta^2$.

When we consider $H(r_{ij} < r_\alpha)$ and $M(r_{ij} < r_\alpha)$, we find that $N_q = H_0 - M_0 = 0$ even for attractive polymer packings that are hypostatic. However, we find that $H_0(r_{ij} < r_\beta) > H_0(r_{ij} < r_\alpha)$ for attractive polymer packings with missing contacts. Therefore, for attractive polymer packings, we count the number of quartic modes N_q as the number of nontrivial zero modes in $H(r_{ij} < r_\beta)$. When including these N_q quartic modes, we find that $\Delta N = N_c(r_{ij} < r_\beta) + N_b + N_q$ versus $V_r N^3$ obeys the same power-law scaling and finite-size collapse as packings of repulsive disks, repulsive polymers, and attractive disks. [See Fig. 8(d).] While packings of attractive polymers are effectively isostatic, we also find that the

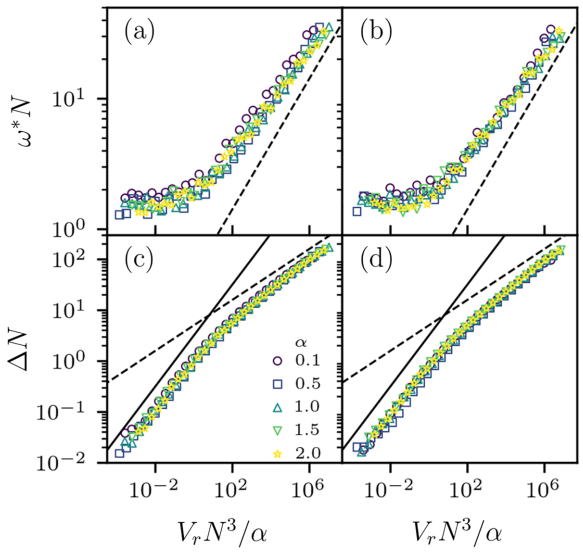

FIG. 12. Characteristic plateau frequency of the vibrational density of states ω^* plotted versus $V_r N^3/\alpha$ for attractive (a) disk and (b) polymer packings and the excess contacts ΔN plotted versus $V_r N^3/\alpha$ for attractive (c) disk $[\Delta N = N_c(r_{ij} < r_\beta) - N_c^{\rm iso}]$ and (d) polymer $[\Delta N = N_c(r_{ij} < r_\beta) + N_b + N_q - N_c^{\rm iso}]$ packings and with varying attractive ranges, $\alpha = 0.1$ (circles), 0.5 (squares), 1.0 (upward triangles), 1.5 (downward triangles), and 2.0 (stars) colored purple to yellow with increasing α for $N = 256$. In (a) and (b), the dashed lines indicate slopes of $1/4$ and in (c) and (d) the dashed and solid lines indicate slopes of $1/4$ and $1/2$ respectively.

low-frequency eigenvalues of the stiffness matrix $h^i(r_{ij} < r_\beta)$ deviate from those $h^i(r_{ij} < r_\alpha)$ defined using the full attractive potential [Fig. 10(b)]. This result indicates that quartic modes in attractive polymer packings are more sensitive (compared to the low-frequency stiffness matrix eigenvalues of packings of attractive disks) to the addition of the weak long-range attractions of the full attractive potential.

Are attractive disks and polymers still effectively isostatic when varying the range of the attractive interaction α? We change the attractive range in small steps, $\alpha = \alpha_0 \pm \Delta\alpha$, where $\alpha_0 = 1.5$ and $\Delta\alpha = 0.01$ with each α increment followed by overdamped energy minimization. In Figs. 12(a) and 12(b), we show the scaling of $\omega^* N$ versus $V_r N^3/\alpha$ for $0.1 \leqslant \alpha \leqslant 2$ for packings of attractive disks and polymers and find that $\omega^* N \sim (V_r N^3/\alpha)^{1/4}$ collapses the data for all values of α. In Fig. 12(c) and 12(d), we show that packings of attractive disks and polymers are also effectively isostatic when defining contacts according to $r_{ij} < r_\beta$ for all α. For all packings of attractive disks and polymers, $\Delta N > 0$ and ΔN versus $V_r N^3/\alpha$ obeys the same scaling relation as that found for isostatic packings of repulsive disks and polymers.

IV. CONCLUSIONS AND FUTURE DIRECTIONS

In this work, we studied the connection between the collapse of attractive disk-shaped bead-spring polymers and the onset of jamming in packings of repulsive disks and polymers. This work was motivated by the fact that protein cores possess similar packing fractions to those of jammed packings of purely repulsive, disconnected amino-acid-shaped particles. Is there a deep connection between attractive polymer collapse and compression-induced jamming or is the similarity fortuitous?

First, we showed that for packings of attractive disk-shaped bead-spring polymers to possess interior packing fractions similar to those in jammed repulsive disk packings, they must be quenched to temperatures much below the glass transition temperature. To compare packings of attractive and repulsive disks and polymers, we developed a method to compress repulsive systems under open boundary conditions. We find that the average core packing fraction of repulsive disk and polymer packings under this protocol is similar to that generated by thermally quenching attractive disks and polymers.

Previous studies have shown that repulsive disk packings at jamming onset are isostatic leading to an excess of low-frequency modes in the vibrational density of states, with a characteristic plateau frequency $\omega^* \sim \Delta N \sim (V_r N^3)^{1/4}$, where ΔN is the excess contact number, $\Delta N = N_c + N_w - N_c^{\rm iso}$, V_r is the repulsive contribution to the potential energy, N_c is the number of interparticle contacts, N_w is the number of particle-wall contacts, and $N_c^{\rm iso} = 2(N - N_r) + f(d) + 1$. While repulsive polymer packings are typically hypostatic at jamming onset with fewer contacts than degrees of freedom, the number of missing contacts equals the number of quartic modes N_q and we find that repulsive polymers are effectively isostatic such that the excess contacts $\Delta N = N_c + N_w + N_b + N_q - N_c^{\rm iso}$ versus $V_r N^3$ obeys the same scaling form as that found for packings of repulsive disks, where N_b is the number of polymer bonds and $N_c^{\rm iso} = 2(N - N_f) + f(d) + 1$.

In overconstrained systems, the vibrational density of states $D(\omega) \to 0$ in the low-frequency limit [24]. Here we show that even though attractive disk and polymer packings are highly hyperstatic due to longer-range attractive interactions, they possess a plateau in the low-frequency region of $D(\omega)$ and that $\omega^* \sim (V_r N^3)^{1/4}$. Since this power-law scaling behavior for ω^* versus $V_r N^3$ is similar to that for packings of repulsive disks and polymers near jamming onset, it suggests that packings of attractive monomers and polymers with weak attractions are effectively isostatic. We find that if we define contacts as nonbonded pairs with $r_{ij} < r_\beta$, packings of attractive monomers and polymers are effectively isostatic with $\Delta N = N_c(r_{ij} < r_\beta) + N_q - N_c^{\rm iso} \sim (V_r N^3)^{1/4}$, where $N_c^{\rm iso} = 2N - f(d)$. These results indicate that longer-range attractions provide an average compression force, but that the mechanical properties are controlled by the stronger short-range repulsive interactions.

Overall, we find that there is a deep connection between the interior packing fraction, low-frequency regions of the vibrational density of states, and isostaticity in all four systems: jammed packings of repulsive disks and polymers and thermally quenched, collapsed attractive disks and polymers. Note that we considered an interparticle potential with a discontinuous jump in its second derivative, and the location of the discontinuity corresponded to the definition of interparticle contacts that yields effective isostaticity. In future work, we will study interaction potentials where we can vary the magnitude of the jump in the second derivative and the range over which it changes to understand the parameters that control whether attractive packings can be considered as effectively isostatic. In addition, many biological polymers, such as

proteins, have varying attractive strengths between monomers. We anticipate that we will find similar results for polymers with monomers that have varying attractive strengths, as found here for monomers with uniform attractions. Varying attraction strengths will cause more frustration during polymer collapse and will be considered in future studies.

Here we established that for thermally quenched attractive disk-shaped bead-spring polymers to obtain interior packing fractions near values found for jammed packings of repulsive disks and polymers, they must be cooled below the glass transition temperature. Thus, the collapsed polymers we considered are glassy and the interior packing fraction can be increased by decreasing the cooling rate [45]. Similarly, we have already shown that the packing fraction at jamming onset for packings of repulsive amino-acid-shaped particles spans the range $0.55 < \phi < 0.62$, where the average core packing fraction for protein x-ray crystal structures ($\langle\phi\rangle \sim 0.55$) is only obtained in the limit of rapid compression and energy minimization [16]. In contrast, the current view of the dynamics of protein folding suggests that it is an equilibrium process, akin to finding the global minimum in the potential energy landscape [46–49].

Our work suggests that experimentally determined protein cores can in principle reach packing fractions of $\phi = 0.62$ and yet we find that they always possess the rapid thermal quench value of $\phi \sim 0.55$. Additionally, the approach developed here suggests that isostatic arguments can be used to understand the experimentally measured excess low-frequency content in the vibrational density of states from x-ray scattering studies of proteins [20–23]. In future work, we will generate static packings of single proteins using an all-atom hard-sphere model for proteins with stereochemical constraints (including constraints on the bond lengths, bond angles, and peptide bond dihedral angles ω) using compression or thermal collapse with short-range attractive interactions, to determine whether the cores in these model proteins can possess a range of packing fractions. These single protein packings will obey the geometric criteria of high-quality x-ray crystal structures of proteins (i.e., no nonbonded overlaps and bond lengths, bond angles, and backbone and side-chain dihedral angles will obey the statistics found for protein structures in the Protein Data Bank) and will identify the range of mechanically stable packing fractions in protein cores.

ACKNOWLEDGMENTS

The authors acknowledge support from NIH Training Grant No. T32GM145452 and the High Performance Computing facilities operated by Yale's Center for Research Computing.

APPENDIX A: PACKING-GENERATION PROTOCOL

In this Appendix, we provide details for the packing-generation process for all four systems: jammed packings of repulsive disks, of repulsive polymers, of attractive disks, and of attractive polymers. To initialize all four systems, we first simulate liquid globule configurations of collapsed attractive polymers. We then generate static packings using damped MD simulations.

1. Preparing initial configurations via polymer collapse

To generate initial configurations, we simulate bead-spring polymers with nonbonded attractive interactions over a range of temperatures using a Langevin thermostat. We integrate Newton's equations of motion for each monomer position $\vec{r}_j$ using a modified velocity-Verlet integration scheme with timestep $\Delta t = 0.01$ [50]. We characterize the temperature-dependent polymer configurations using the normalized radius of gyration:

$$\widetilde{R}_g = \frac{R_g - R_g^{\min}}{R_g^{\max} - R_g^{\min}}, \tag{A1}$$

where $R_g^{\max}$ and $R_g^{\min}$ are the maximum and minimum radii of gyration over the course of the simulation, shown in Fig. 13(a) for $N = 256$ and averaged over 100 different initial conditions. Polymers with attractive nonbonded interactions undergo two distinct transitions as they are cooled from high to low temperatures. At high temperatures, the polymer samples an excluded-volume random walk. As the temperature is lowered, the attractive interactions overcome thermal fluctuations, and the polymer collapses into a condensed droplet, signaling the coil-to-globule transition. We fit a sigmoidal curve to the normalized radius of gyration,

$$\widetilde{R}_g(T) = \frac{1}{1 + e^{\kappa(T - T_m)}}, \tag{A2}$$

to identify the melting temperature T_m [51] at which $\widetilde{R}_g(T_m) = 1/2$ and where κ gives the transition width. By cooling the polymer below T_m, we can induce a glass transition, where the structural relaxation time τ_r of the monomers in the globule diverges. We determine τ_r by calculating the self-part of the intermediate scattering function,

$$F_s(q,t) = \frac{1}{N}\left\langle \sum_{j=1}^{N} e^{i\vec{q}\cdot(\vec{r}_j(t_0+t) - \vec{r}_j(t_0))} \right\rangle, \tag{A3}$$

as a function of time t. The angle brackets indicate an average over time origins t_0 and directions of the wave number with magnitude $q = 2\pi/\sigma_{\max}$. As shown in Fig. 13(b), at short times, $F_s(q,t) \sim 1$ since the monomer positions are similar to what they were at the time origin. $F_s(q,t)$ decays to zero when the configuration at time t is uncorrelated with the initial configuration. We define the structural relaxation time τ_r using $F_s(q,\tau_r) = 1/e$, which increases rapidly as the temperature decreases. We can estimate the glass transition temperature T_g at which $\tau_r \to \infty$ using a power-law, $\tau_r \propto (T - T_g)^{-\eta}$ (with $\eta \approx 2$), or super-Arrhenius form, $\tau_r \propto e^{A/(T - T_g)}$ (with $A \approx 10$). Both forms give $T_g/T_m \approx 0.14$, as shown in Fig. 13(c). The results in Fig. 13 are shown for an interparticle potential with attractive range $\alpha = 1.5$ and depth $\beta = 10^{-5}$. We find qualitatively similar results for a range of α and β. Increasing β shifts the melting curve to larger values of temperature, while increasing α broadens the coil-to-globule transition [52].

We first generate extended polymer configurations at high temperature $T \gg T_m$. We then slowly cool the polymers to temperatures T_0 below T_m, i.e., $T_0/T_m = 0.43$, 0.32, and 0.27, but above T_g, as shown in Fig. 13(a) as vertical dotted lines. We collect between 10^2 and 10^3 distinct sets of positions and

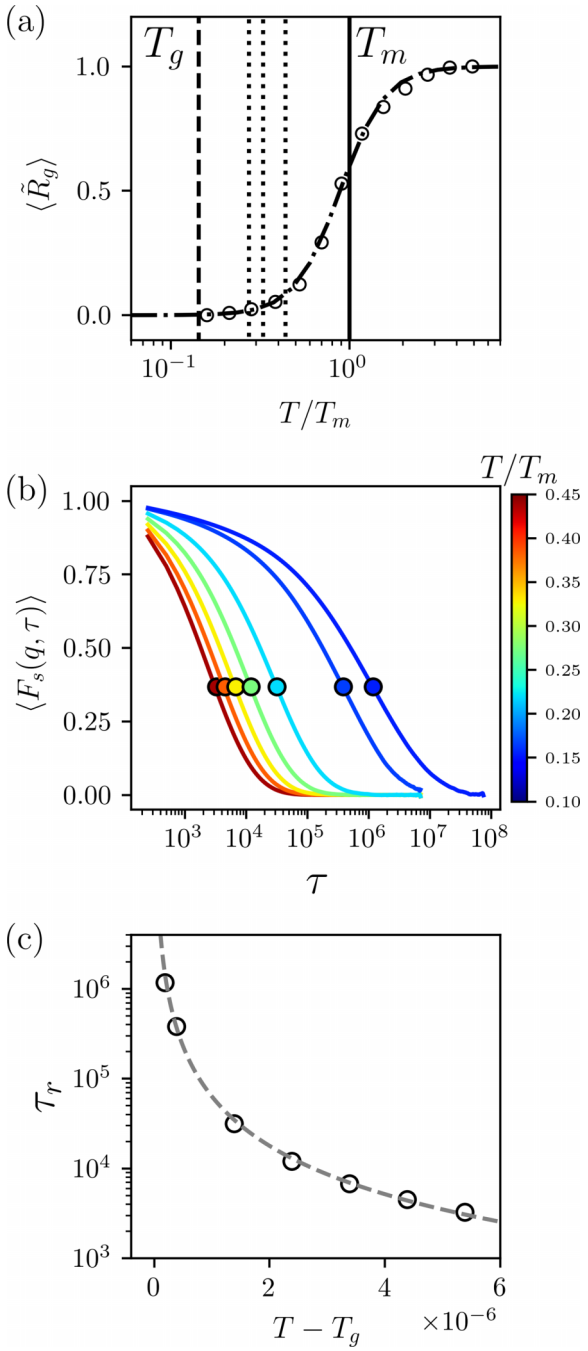

FIG. 13. (a) Normalized radius of gyration $\widetilde{R}_g$ plotted versus temperature T normalized by the melting temperature T_m (vertical solid black line). The dot-dashed line gives the fit of $\widetilde{R}_g$ to Eq. (A2). (b) The self-part of the intermediate scattering function $F_s(q,t)$ at $q\sigma_s = 2\pi\sigma_s/\sigma_{\max}$ averaged over all particles and time origins for several T/T_m. The filled circles indicate the structural relaxation times τ_r at which $F_s(q,\tau_r) = 1/e$. The colors from red to blue indicate high to low values of T/T_m. The vertical dashed line in (a) indicates T_g below which $\tau_r \to \infty$. (c) The structural relaxation time τ_r plotted versus the deviation in the temperature from the glass transition $T - T_g$, where T_g is found via a power-law fit (gray dashed line).

velocities of the polymers at each T_0, with each set separated by $10\tau_r$. We consider $N = 64$, 128, 256, 512, and 1024 to assess system-size effects. After generating the collapsed polymer configurations, we follow the protocols below to generate zero-temperature packings of polymers with nonbonded attractive interactions, disk packings with attractive interactions, packings of polymers with only nonbonded repulsive interactions, and disk packings with only repulsive interactions.

2. Packing-generation protocol for attractive disks and polymers

To generate static packings of attractive polymers, we cool liquid globules at T_0 to zero temperature using damped MD simulations, where we solve Newton's equations of motion,

$$m\vec{a}_j = -\partial V/\partial \vec{r}_j - b\vec{v}_j, \tag{A4}$$

with dissipative forces proportional to the disk velocities $\vec{v}_j$, potential energy $V = V^b + V^{\rm anb}$, disk mass m and acceleration $\vec{a}_j$, and $j = 1, \ldots, N$ labels the disks. For computational efficiency, each system is cooled using the reported damping parameter b until the total force magnitude in the system reaches $F_{\rm tol} = \Sigma_{j=1}^{N} |\vec{F}_j| < 10^{-7}$, where $\vec{F}_j = \sum_i \vec{f}_{ij}$ is the total force on particle j due to interactions with neighboring particles i $\vec{f}_{ij}$. The damping parameter is then increased to $b = 0.1$ in the overdamped limit and the force tolerance is decreased to $F_{\rm tol} < 10^{-15}$.

The damped MD simulations can be performed on attractive disks (as well as attractive polymers) to investigate the effect of the polymer backbone on the zero-temperature packings. To generate static packings of attractive disks, we initialize the system with the positions and velocities of the collapsed polymer globules at T_0 and then use damped MD simulations [Eq. (A4)] to minimize the total potential energy, except now $V = V^{\rm anb}$.

3. Packing-generation protocol for purely repulsive disks and polymers

For systems with attractive interactions, we employ open boundary conditions. Since static packings of purely repulsive particles possess nonzero pressures at jamming onset, they must be confined to form jammed packings, e.g., using periodic or fixed boundary conditions. To generate jammed packings of purely repulsive particles in *open* boundary conditions, we include a linear spring potential that connects each particle to the center of mass of the packing, which is the origin of the coordinate system,

$$\frac{V^c(r_i)}{\epsilon} = \frac{k_c}{2\epsilon} r_i^2 (\sigma_i/\sigma_{\max})^{\nu}, \tag{A5}$$

where $k_c\sigma_s^2 \ll \epsilon$ is the compressive energy scale. (See Appendix B for a discussion of how the results depend on k_c/ϵ.) To generate zero-temperature packings of purely repulsive particles, we initialize the system with the positions and velocities from the collapsed globules at T_0. We then run damped MD simulations with $V = V^b + V^{\rm rnb} + V^c$ for purely repulsive polymers or $V = V^{\rm rnb} + V^c$ for purely repulsive monomers until force balance is achieved. The radial spring is then removed and the packings are again energy minimized until $F_{\rm tol} < 10^{-15}$. For small damping coefficients, packings of repulsive disks with similar sizes segregate and crystallize. We thus include a factor of $(\sigma_i/\sigma_{\max})^{\nu}$ with $\nu = 2$

in Eq. (A5) to prevent size segregation during compression. (See Appendix B.)

To calculate the structural and mechanical properties of disk and polymer packings with purely repulsive interactions as a function of the packing fraction above jamming onset, we add a repulsive circular boundary with radius R via the repulsive linear spring potential,

$$\frac{V^w(r_i)}{\epsilon} = \frac{1}{2}\left(1 - \frac{R - r_i}{\sigma_i}\right)^2 \Theta\left(1 - \frac{R - r_i}{\sigma_i}\right). \tag{A6}$$

R is initialized so that there are no disk-wall contacts. The system is successively compressed by scaling the wall and particle positions such that $r_i' = r_i(1 - 2\Delta\phi/\phi)$ with each compression step $\Delta\phi = 10^{-3}$ followed by energy minimization using damped MD simulations with $b = 0.1$. The system is compressed until it reaches a target total potential energy per particle $V_0 < V/N < 2V_0$. If the system is compressed above $V/N > 2V_0$, then the previous particle positions and boundary radius are reinitialized, and the system is compressed by $\Delta\phi/2$ and energy minimized. The static packings were prepared over a wide range of potential energies per particle, $10^{-13} \lesssim V_0 \lesssim 10^{-2}$.

4. Core packing fraction

To analyze the structural properties of the interiors of static packings, their surfaces must first be identified. To do this, we adapt and apply an algorithm first proposed for finding the surfaces of proteins in solvent from Lee and Richards [53]. In the case of disk and polymer packings in open boundaries, we place a probe disk of diameter σ_p on the "anchor" disk that is furthest from the center of mass of the packing. We rotate the probe around the anchor disk in angle increments of $\Delta\theta = 0.1$ radians and check for overlaps with neighboring disks. If a new contact is made with the probe disk, then the new contacting disk becomes the anchor disk. This process is repeated until the probe disk returns to the initial anchor disk.

The size of the probe will determine which disks are labeled as core and thus σ_p affects the average core packing fraction $\langle\phi\rangle$. In Fig. 14, we plot $\langle\phi\rangle$ versus σ_p for $N = 256$ attractive polymer packings. For large probe sizes, similar in size to the largest disk in the system, the core packing fraction decreases significantly as more surface-like (noncore) particles are included in the average. The core packing fraction plateaus as $\sigma_p \lesssim 0.4$. The typical probe size used to study proteins is the diameter of a water molecule $\sigma_p \sim 2.8$ Å, whereas the maximum diameter of an alanine residue is 6.6 Å, which yields the ratio, $\sigma_p/\sigma_s \sim 0.43$. In the studies in the main text, we chose a similar ratio $\sigma_p/\sigma_s = 0.1$.

After identifying the surface disks of a given configuration, a radical Voronoi tessellation is performed on the disk centers within a square box with an edge length exceeding the largest extent of each packing [54]. The core packing fraction for a particular configuration is defined as

$$\phi = \frac{\sum_{i=1}^{N_c} \pi\sigma_i^2/4}{\sum_{i=1}^{N_c} a_i}, \tag{A7}$$

where N_c is the number of core disks and a_i the area of the Voronoi polygon surrounding the ith core disk. Due to the small probe radius, all of the core disks have closed Voronoi cells and so their areas do not depend on the enclosing box size.

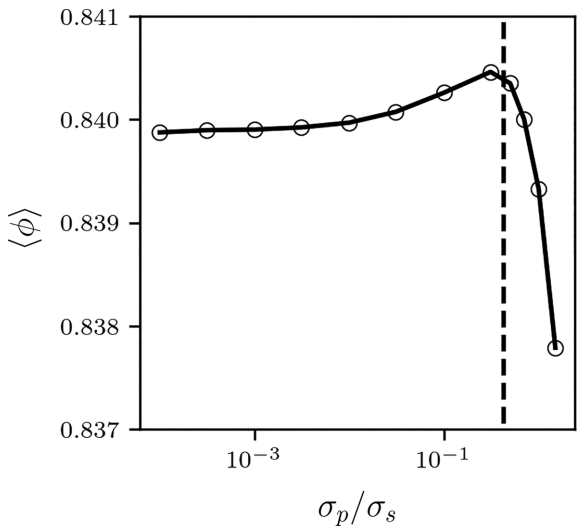

FIG. 14. The average core packing fraction $\langle\phi\rangle$ plotted versus the ratio of the surface probe diameter to the smallest disk diameter σ_p/σ_s for packings of attractive polymers with $N = 256$, $b = 10^{-5}$, and $T_0/T_m = 0.27$. The vertical dashed line indicates $\sigma_p/\sigma_s \sim 0.43$, which is the ratio of the diameter of a water molecule to an alanine residue.

APPENDIX B: GENERATING AMORPHOUS PACKINGS OF REPULSIVE PARTICLES IN OPEN BOUNDARY CONDITIONS

To generate static packings of repulsive disks and polymers under open boundary conditions, we apply an external central

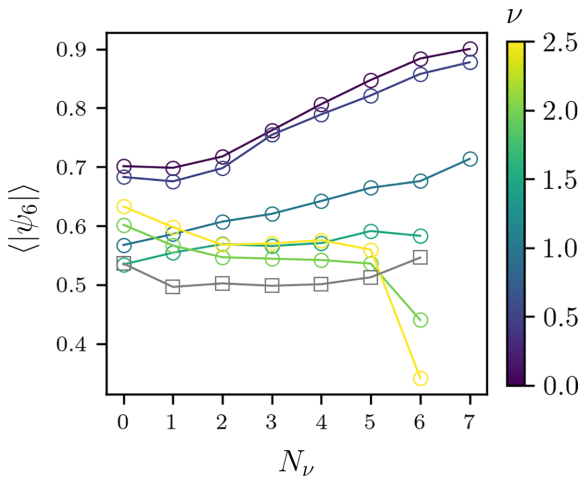

FIG. 15. The average hexatic order parameter $\langle|\psi_6|\rangle$ plotted versus the number of Voronoi cells N_ν between each disk and the closest surface disk for varying exponents ν (increasing from purple to yellow) that control the strength of the bias factor of the compression force for packings of repulsive disks with $N = 256$ prepared using $b = 10^{-5}$. As a comparison, we also show results for packings of attractive disks prepared at the same value of b (gray squares).

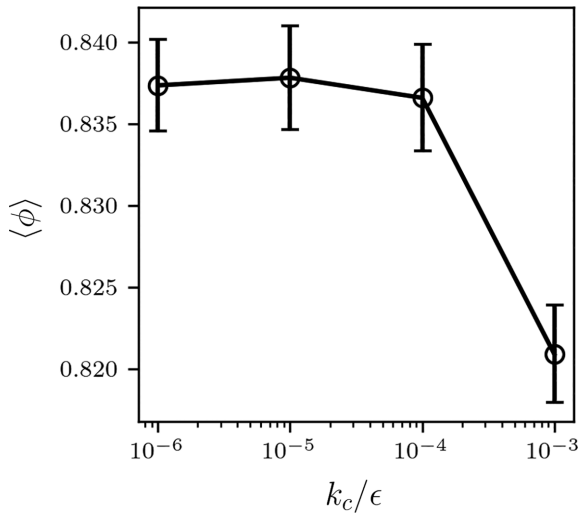

FIG. 16. The average core packing fraction $\langle\phi\rangle$ of packings of repulsive disks plotted as a function of k_c/ϵ using $N = 256$ and $b = 0.1$.

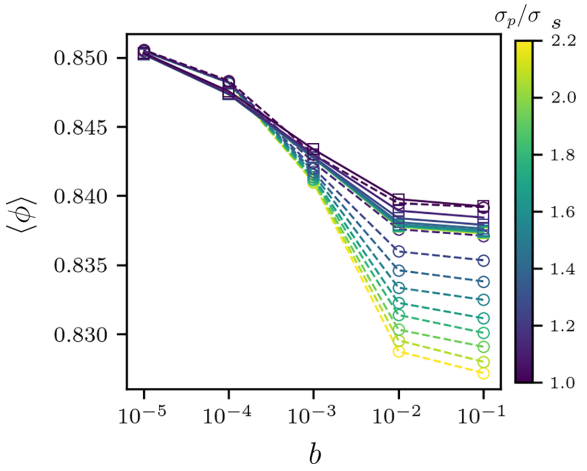

FIG. 17. The average core packing fraction $\langle\phi\rangle$ from damped MD simulations of attractive polymers initialized at $T_0/T_m = 0.43$ (circles with dashed lines) and 0.27 (squares with dashed lines) plotted versus the damping parameter b when void regions are identified using probe diameters, $2.2 \lesssim \sigma_p/\sigma_s < 1$ (where purple to yellow indicates increasing size), for $N = 512$. Core disks adjacent to void regions are not included in the calculation of $\langle\phi\rangle$.

potential V^c in Eq. (A5) for all disks in the packing. With this central potential and in the limit of large damping paramaters, repulsive disk and polymer packings are highly disordered. However, with low damping parameters, thermal fluctuations can induce size segregation in packings of repulsive disks, with small disks slipping past large disks, which leaves only large disks on the surface and gives rise to crystallization. Therefore, we add a bias factor $(\sigma_i/\sigma_{\max})^\nu$ to the compression force, such that larger disks feel larger compression forces. The exponent ν controls the strength of the bias factor.

As shown in Fig. 5(b), attractive disk and polymer packings do not size segregate and therefore we can calibrate the value of ν by comparing the structural properties of repulsive disk packings to those of attractive disk and polymer packings. In Fig. 15, we plot the average hexatic order parameter $\langle|\psi_6|\rangle$ [Eq. (4)] versus the number N_v of Voronoi cells between a disk and the surface as a function of ν for packings of repulsive disks. As ν increases, the hexactic order decreases strongly for all values of N_v. However, the similarity between the repulsive and attractive disk packings decreases when $\nu \gtrsim 2.5$. Therefore, we use $\nu = 2$ for preparing all repulsive disk packings in these studies.

We also studied the influence of the spring constant k_c/ϵ on the core packing fraction in packings of repulsive disks. The spring constant k_c controls the effective rate of compression, which is known to influence the structural properties of jammed packings [24]. In Fig. 16, we plot the average core packing fraction $\langle\phi\rangle$ for 100 repulsive disk packings for $N = 256$ and $b = 0.1$ versus k_c/ϵ. When compressing with large k_c/ϵ, the repulsive disk packings tend to be less densely packed and the packing fraction reaches a plateau for $k_c/\epsilon \lesssim 10^{-4}$. Therefore, we selected $k_c/\epsilon = 10^{-4}$ to generate all repulsive disk and polymer packings.

APPENDIX C: IDENTIFICATION OF VOID REGIONS

The core packing fraction for collapsed, attractive polymers is minimal for high damping parameters b and high initial temperatures T_0. We find that these collapsed structures possess large void regions surrounded by regions that are densely packed. To identify the void regions, we test each interior disk to determine whether a probe disk of diameter σ_p can be placed at its edge without causing any overlaps. If the probe can be placed without causing overlaps, then we remove that disk from the list of core disks. In Fig. 17, we show that when we remove core disks that are near void regions (by choosing $\sigma_p/\sigma_s = 1$), the core packing fraction $\langle\phi\rangle$ is no longer strongly dependent on T_0 for high damping parameters. Since the collapsed structures in the low damping limit do not possess void regions, $\langle\phi\rangle$ does not depend on T_0 or σ_p for small b. Thus, aside from void regions, the initial temperature has only a minor effect on the packing fraction of dense core regions of collapsed, attractive polymers.

[1] F. M. Richards, The interpretation of protein structures: Total volume, group volume distributions and packing density, J. Mol. Biol. **82**, 1 (1974).
[2] C. Chothia, Structural invariants in protein folding, Nature (Lond.) **254**, 304 (1975).
[3] F. M. Richards, Areas, volumes, packing, and protein structure, Annu. Rev. Biophys. Bioeng. **6**, 151 (1977).
[4] J. Tsai, R. Taylor, C. Chothia, and M. Gerstein, The packing density in proteins: Standard radii and volumes, J. Mol. Biol. **290**, 253 (1999).
[5] J. Liang and K. A. Dill, Are proteins well-packed? Biophys. J. **81**, 751 (2001).
[6] J. C. Gaines, W. W. Smith, L. Regan, and C. S. O'Hern, Random close packing in protein cores, Phys. Rev. E **93**, 032415 (2016).

[7] A. T. Grigas, Z. Liu, L. Regan, and C. S. O'Hern, Core packing of well-defined x-ray and NMR structures is the same, Protein Sci. **31**, e4373 (2022).

[8] K. A. Dill, Dominant forces in protein folding, Biochemistry **29**, 7133 (1990).

[9] J. Xu, W. A. Baase, E. Baldwin, and B. W. Matthews, The response of T4 lysozyme to large-to-small substitutions within the core and its relation to the hydrophobic effect, Protein Sci. **7**, 158 (1998).

[10] W. A. Baase, L. Liu, D. E. Tronrud, and B. W. Matthews, Lessons from the lysozyme of phage T4, Protein Sci. **19**, 631 (2010).

[11] C. N. Pace, H. Fu, K. L. Fryar, J. Landua, S. R. Trevino, B. A. Shirley, M. M. Hendricks, S. Iimura, K. Gajiwala, J. M. Scholtz, and G. R. Grimsley, Contribution of hydrophobic interactions to protein stability, J. Mol. Biol. **408**, 514 (2011).

[12] A. T. Grigas, Z. Mei, J. D. Treado, Z. A. Levine, L. Regan, and C. S. O'Hern, Using physical features of protein core packing to distinguish real proteins from decoys, Protein Sci. **29**, 1931 (2020).

[13] J. C. Gaines, A. H. Clark, L. Regan, and C. S. O'Hern, Packing in protein cores, J. Phys.: Condens. Matter **29**, 293001 (2017).

[14] J. C. Gaines, S. Acebes, A. Virrueta, M. Butler, L. Regan, and C. S. O'Hern, Comparing side chain packing in soluble proteins, protein-protein interfaces and transmembrane proteins, Proteins: Struct. Funct. Bioinf. **86**, 581 (2018).

[15] J. D. Treado, Z. Mei, L. Regan, and C. S. O'Hern, Void distributions reveal structural link between jammed packings and protein cores, Phys. Rev. E **99**, 022416 (2019).

[16] Z. Mei, J. D. Treado, A. T. Grigas, Z. A. Levine, L. Regan, and C. S. O'Hern, Analyses of protein cores reveal fundamental differences between solution and crystal structures, Proteins: Struct. Funct. Bioinf. **88**, 1154 (2020).

[17] D. Seeliger and B. L. de Groot, Atomic contacts in protein structures. A detailed analysis of atomic radii, packing, and overlaps, Proteins: Struct. Funct. Bioinf. **68**, 595 (2007).

[18] H. Yamada, T. Nagae, and N. Watanabe, High-pressure protein crystallography of hen egg-white lysozyme, Acta Crystallogr. D **71**, 742 (2015).

[19] T. Nagae, H. Yamada, and N. Watanabe, High-pressure protein crystal structure analysis of *Escherichia coli* dihydrofolate reductase complexed with folate and $NADP^+$, Acta Crystallogr. D **74**, 895 (2018).

[20] S. Perticaroli, J. D. Nickels, G. Ehlers, H. O'Neill, Q. Zhang, and A. P. Sokolov, Secondary structure and rigidity in model proteins, Soft Matter **9**, 9548 (2013).

[21] S. Perticaroli, J. D. Nickels, G. Ehlers, and A. P. Sokolov, Rigidity, secondary structure, and the universality of the Boson peak in proteins, Biophys. J. **106**, 2667 (2014).

[22] H. Nakagawa, Y. Joti, A. Kitao, O. Yamamuro, and M. Kataoka, Universality and structural implications of the Boson peak in proteins., Biophys. J. **117**, 229 (2019).

[23] T. Mori, Y. Jiang, Y. Fujii, S. Kitani, H. Mizuno, A. Koreeda, L. Motoji, H. Tokoro, K. Shiraki, Y. Yamamoto, and S. Kojima, Detection of Boson peak and fractal dynamics of disordered systems using terahertz spectroscopy, Phys. Rev. E **102**, 022502 (2020).

[24] C. S. O'Hern, L. E. Silbert, A. J. Liu, and S. R. Nagel, Jamming at zero temperature and zero applied stress: The epitome of disorder, Phys. Rev. E **68**, 011306 (2003).

[25] L. E. Silbert, A. J. Liu, and S. R. Nagel, Vibrations and diverging length scales near the unjamming transition, Phys. Rev. Lett. **95**, 098301 (2005).

[26] M. Wyart, L. E. Silbert, S. R. Nagel, and T. A. Witten, Effects of compression on the vibrational modes of marginally jammed solids, Phys. Rev. E **72**, 051306 (2005).

[27] A. J. Liu and S. R. Nagel, The jamming transition and the marginally jammed solid, Annu. Rev. Condens. Matter Phys. **1**, 347 (2010).

[28] C. P. Goodrich, S. Dagois-Bohy, B. P. Tighe, M. van Hecke, A. J. Liu, and S. R. Nagel, Jamming in finite systems: Stability, anisotropy, fluctuations, and scaling, Phys. Rev. E **90**, 022138 (2014).

[29] G. Lois, J. Blawzdziewicz, and C. S. O'Hern, Jamming transition and new percolation universality classes in particulate systems with attraction, Phys. Rev. Lett. **100**, 028001 (2008).

[30] D. J. Koeze and B. P. Tighe, Sticky matters: Jamming and rigid cluster statistics with attractive particle interactions, Phys. Rev. Lett. **121**, 188002 (2018).

[31] D. J. Koeze, L. Hong, A. Kumar, and B. P. Tighe, Elasticity of jammed packings of sticky disks, Phys. Rev. Res. **2**, 032047 (2020).

[32] M. Ozawa, L. Berthier, and D. Coslovich, Exploring the jamming transition over a wide range of critical densities, SciPost Phys. **3**, 027 (2017).

[33] S. M. Soik and T. A. Sharp, Effects of spherical confinement and backbone stiffness on flexible polymer jamming, Phys. Rev. E **99**, 052505 (2019).

[34] A. Donev, R. Connelly, F. H. Stillinger, and S. Torquato, Underconstrained jammed packings of nonspherical hard particles: Ellipses and ellipsoids, Phys. Rev. E **75**, 051304 (2007).

[35] C. F. Schreck, M. Mailman, B. Chakraborty, and C. S. O'Hern, Constraints and vibrations in static packings of ellipsoidal particles, Phys. Rev. E **85**, 061305 (2012).

[36] S. Vivek, C. P. Kelleher, P. M. Chaikin, and E. R. Weeks, Long-wavelength fluctuations and the glass transition in two dimensions and three dimensions, Proc. Natl. Acad. Sci. USA **114**, 1850 (2017).

[37] Q. Liao, L. Berthier, H.-J. Zhou, and N. Xu, Dynamic Gardner cross-over in a simple glass, Proc. Natl. Acad. Sci. USA **120**, e2218218120 (2023).

[38] C. F. Schreck, C. S. O'Hern, and L. E. Silbert, Tuning jammed frictionless disk packings from isostatic to hyperstatic, Phys. Rev. E **84**, 011305 (2011).

[39] Q. Wu, T. Bertrand, M. D. Shattuck, and C. S. O'Hern, Response of jammed packings to thermal fluctuations, Phys. Rev. E **96**, 062902 (2017).

[40] H. A. Makse, D. L. Johnson, and L. M. Schwartz, Packing of compressible granular materials, Phys. Rev. Lett. **84**, 4160 (2000).

[41] P. Wang, S. Zhang, P. Tuckman, N. T. Ouellette, M. D. Shattuck, and C. S. O'Hern, Shear response of granular packings compressed above jamming onset, Phys. Rev. E **103**, 022902 (2021).

[42] N. C. Karayiannis, K. Foteinopoulou, and M. Laso, The structure of random packings of freely jointed chains of tangent hard spheres, J. Chem. Phys. **130**, 164908 (2009).

[43] N. C. Karayiannis and M. Laso, Dense and nearly jammed random packings of freely jointed chains of tangent hard spheres, Phys. Rev. Lett. **100**, 050602 (2008).

[44] N. Xu, M. Wyart, A. J. Liu, and S. R. Nagel, Excess vibrational modes and the Boson peak in model glasses, Phys. Rev. Lett. **98**, 175502 (2007).

[45] X. Hu, L. Hong, M. Dean Smith, T. Neusius, X. Cheng, and J. C. Smith, The dynamics of single protein molecules is non-equilibrium and self-similar over thirteen decades in time, Nat. Phys. **12**, 171 (2016).

[46] J. D. Bryngelson and P. G. Wolynes, Spin glasses and the statistical mechanics of protein folding, Proc. Natl. Acad. Sci. USA **84**, 7524 (1987).

[47] P. E. Leopold, M. Montal, and J. N. Onuchic, Protein folding funnels: A kinetic approach to the sequence-structure relationship, Proc. Natl. Acad. Sci. USA **89**, 8721 (1992).

[48] J. N. Onuchic, Z. Luthey-Schulten, and P. G. Wolynes, Theory of protein folding: The energy landscape perspective, Annu. Rev. Phys. Chem. **48**, 545 (1997).

[49] S. S. Plotkin and J. N. Onuchic, Understanding protein folding with energy landscape theory part I: Basic concepts, Q. Rev. Biophys. **35**, 111 (2002).

[50] M. P. Allen and D. J. Tildesley, *Computer Simulation of Liquids*, 2nd ed. (Oxford University Press, Oxford, 2017).

[51] C. Williams, F. Brochard, and H. L. Frisch, Polymer collapse, Annu. Rev. Phys. Chem. **32**, 433 (1981).

[52] W. Paul and M. Müller, Enhanced sampling in simulations of dense systems: The phase behavior of collapsed polymer globules, J. Chem. Phys. **115**, 630 (2001).

[53] B. Lee and F. Richards, The interpretation of protein structures: Estimation of static accessibility, J. Mol. Biol. **55**, 379 (1971).

[54] C. Rycroft, Voro^{++}: A three-dimensional Voronoi cell library in C^{++} (2009), https://www.osti.gov/biblio/946741.